

Efficient synthesis of 3-methylindole using biomass-derived glycerol and aniline over ZnO and CeO₂ modified Ag/SBA-15 catalysts



Yi Qu, Yining Gao, Shuyi Lin, Lei Shi*

College of Chemistry and Chemical Engineering, Liaoning Normal University, Dalian, 116029 Liaoning, China

ARTICLE INFO

Keywords:

3-Methylindole
Ag/SBA-15 catalyst
ZnO and CeO₂ promoters
Biomass-derived glycerol
Reaction pathway

ABSTRACT

An efficient mesoporous catalyst of Ag/SBA-15 modified with ZnO and CeO₂ was successfully constructed with the purpose of efficiently synthesizing 3-methylindole by biomass-derived glycerol and aniline, which up to 62% yield and 75% selectivity for 3-methylindole were achieved when Ag loading was 1.00 mmol/g⁻¹, ZnO or CeO₂ content was 1.00 or 0.05 mmol/g⁻¹, respectively. And only 3% yield decreased when the catalyst was circulated five times. The characterizations researches on N₂ physical adsorption, Fourier transform infrared (FT-IR), scanning electron microscopy and energy-dispersive X-ray spectroscopy (SEM-EDX), temperature programmed reduction of hydrogen (H₂-TPR), X-ray diffraction (XRD), transmission electron microscopy (TEM), temperature programmed desorption (TPD) of NH₃ and CO₂, thermogravimetric and differential thermal analysis (TG-DTA) indicated that adding the promoter of ZnO to Ag/SBA-15 increased the dispersion of the silver particles significantly and controlled the aggregation of Ag nanoparticles during the reaction remarkably because doping ZnO greatly increased the polarity of the composite carrier SBA-15-ZnO and brought about the interaction between Ag and carrier enhanced. CeO₂ could promote the reduction of Ag₂O and suppress the formation of carbon deposition effectively. In addition, doping ZnO and CeO₂ increased the number of the weak-acid centers of the SBA-15 supported Ag-based catalyst observably, thereby the catalyst of Ag/SBA-15-ZnO-CeO₂ acquired a good selectivity. Moreover, the reaction pathway for 3-methylindole synthesis by biomass-derived glycerol and aniline was probed in depth and a reasonable route was proposed.

1. Introduction

With the increasing shortage of fossil fuels, the efficient use of renewable biomass resources to partially replace fossil fuels has received widespread attention [1–4]. Biodiesel, as one of the typical representatives of biofuels and a green energy source, has the advantages of renewable, degradable, and low pollution [5–7]. And in recent years, the research concerning the production of biodiesel have become of a great interest [8]. However, the production of biodiesel would emerge a large amount of by-product glycerol [9,10]. How to effectively convert biomass-derived glycerol to high value-added chemicals is a topic of great concern to chemical researchers [11], which can improve the sustainability and economic viability of biodiesel production. Delightfully, many value-added chemicals have been successfully produced from biomass-derived glycerol by various methods [12–14]. For example, hydrogenolysis, hydrodeoxygenation, dehydration, etherification, transesterification and polymerization, etc. [15–20].

In our recent study, it has been found that biomass-derived glycerol with aniline could be used as raw materials to synthesize a high value-

added chemical of 3-methylindole [21]. It's well known that indole and its derivatives are important fine chemicals widely used in the production of drug, pesticides, spices and dye [22–26]. 3-Methylindole, a noted compound of indoles, has an extensive application in many fields due to its unique structure. For example, it can be used to prepare antihypertensive drugs, stimulants, analgesics, and anticancer drugs, etc. [27,28].

At present, there are many methods to synthesize 3-methylindole. Among them, the most famous method is the Fischer synthesis. Simoneau et al. [29] reported the Fischer cyclization of 1-nitropropane and phenylhydrazine catalyzed by sulfuric acid and a 50% yield of target product was obtained. Kanchupalli et al. [30] proposed the transannulationin from pyridazine N-oxide and pyrrole to produce 3-methylindole over Rh₂(esp)₂ with the yield of 67%. Moreover, Campanati et al. [31] carried out the catalytic reaction with aniline and 1,2-propanediol as raw materials in a fixed bed at atmospheric pressure over ZrO₂/SiO₂, however 3-methylindole yield was merely 12%. Since there are many disadvantages for the current synthesis of 3-methylindole such as a high cost of reactants or catalysts, a low yield of target

* Corresponding author.

E-mail address: shilei515dl@126.com (L. Shi).

product, a complicated experimental operation or the use of a large amount of toxic solvents, etc, it is therefore, essential to develop an efficient synthesis method of 3-methylindole to meet the requirements of cost-saving as well as environmentally friendly. Using aniline and biomass-derived glycerol as raw materials to synthesize 3-methylindole is in line with the concept of atom economy and is currently the most promising method because of a low cost and environmental friendliness. From our indepth research on the reaction in recent years, it has been found that the catalyst carrier should have a large specific surface area and a large number of weak-acid centers to ensure its high activity and good selectivity [21,32,33].

Mesoporous materials are greatly favored in the field of catalysis due to their unique structure and properties [34,35]. Among them, mesoporous silica SBA-15 is a good alternative as carrier of heterogeneous catalysts [36–38] because of its large specific surface area, good hydrothermal stability, adjustable pore size and regular pore structure, etc [39–42]. And now it has been successfully applied in many catalytic reactions [43–45]. ZnO and CeO₂ additives have excellent promotion effect in many catalytic reactions [46–49]. Therefore, in this work, SBA-15 was proposed as the carrier to prepare the Ag-based catalysts for the catalytic reaction of glycerol and aniline to synthesize 3-methylindole. To improve the performance of the catalyst, ZnO and CeO₂ promoters were added to Ag/SBA-15 catalyst in sequence and the effects of ZnO and CeO₂ were investigated thoroughly by N₂ physical adsorption, FT-IR, SEM-EDX, H₂-TPR, XRD, TEM, NH₃/CO₂-TPD, TG-DTA. The reaction pathway of 3-methylindole synthesis on Ag/SBA-15-ZnO-CeO₂ was further studied meticulously and a reasonable route was proposed.

2. Experimental

2.1. Materials

Silver nitrate (AgNO₃, ≥99.0%), zinc nitrate (Zn(NO₃)₂·6H₂O, ≥99.0%), cerium nitrate (Ce(NO₃)₃·6H₂O, ≥99.0%), aniline (C₆H₅NH₂, ≥99.5%), and n-Hexanol (C₆H₁₃OH, ≥95.0%) were obtained from Tianjin Damao Chemical Reagent Co., Ltd. (China). Tetraethyl orthosilicate (TEOS, (C₂H₅O)₄Si, ≥98.0%), hydrochloric acid (HCl, 36–38%), glycerol (C₃H₈O₃, ≥99.0%), acetol (C₃H₆O₂, > 99.0%) and 1,2-propanediol (C₃H₈O₂, > 99.0%) were obtained from Tianjin Kemiou Chemical Reagent Co., Ltd. (China). Pluronic P123 (Mn = 5800, EO₂₀PO₇₀EO₂₀) were obtained from Beijing Reagent Co., Ltd. (China). The above chemicals were not purified before use.

2.2. Preparation of SBA-15 carrier and silver-based catalysts

SBA-15 carrier was hydrothermally prepared according to the literature [50] with a minor modification. A 4 g of P123 (EO₂₀PO₇₀EO₂₀) was dispersed in 160 mL (1.5 M) hydrochloric acid solution. After the solution was stirred thoroughly with the magnetic stirrer until the surfactant was completely dissolved and uniformly dispersed, a 8.5 g of TEOS was dissolved in the above solution, and stirred at 313 K for 24.0 h using a magnetic stirrer. Then the miscible liquids underwent an additional aging at 353 K for 24.0 h, and the suspension was filtered, washed. The sample was air-dried and calcined at 773 K for 6.0 h in a muffle furnace. Finally, the sample of SBA-15 was obtained. From Fig. 1 it can be known that the SBA-15 carrier was successfully prepared, which had a P6mm symmetrical hexagonal structure [51].

The catalyst of Ag/SBA-15 was obtained by equal volume impregnation method. A certain amount of SBA-15 carrier was soaked into a certain concentration of an aqueous solution of AgNO₃ for 15.5 h in air. After the impregnation, the sample was dried at 393 K, and finally calcined at 773 K for 4.0 h. The catalyst was reduced at 453 K for 2.0 h with a mixture flow of H₂ (15 mL min⁻¹)-N₂ (15 mL min⁻¹) before the catalytic reaction.

The catalyst of Ag/SBA-15-ZnO was synthesized by sequential impregnation. First, a certain amount of SBA-15 carrier was soaked in a certain concentration of aqueous solution of Zn(NO₃)₂ for 15.5 h. After dried at 393 K, the mixture was calcined at 873 K for 4.0 h to obtain SBA-15-ZnO. The active component was then loaded on the modified carrier of SBA-15-ZnO and the process was the same as the preparation of silver catalyst described above.

Ag/SBA-15-ZnO-CeO₂ was also prepared by the same method of sequential impregnation. The process was the same as the preparation of the catalyst of Ag/SBA-15-ZnO.

Ag loading to all the SBA-15 supported silver-based catalysts was 1.00 mmol/g⁻¹.

2.3. Evaluation of catalysts

The catalytic activity and selectivity of Ag-based catalyst were measured in a fixed-bed continuous flow glass reactor. The catalytic reaction was proceeded at 483 K. The space velocity (SV) of the reaction was 1700 h⁻¹, and the liquid hourly space velocity (LHSV) of aniline and glycerol was 0.4 h⁻¹. The reactant solution (glycerol/aniline molar ratio of 1:3) pre-heated in a buffer bottle to evaporate was carried into the catalyst bed with H₂ (15 mL min⁻¹), N₂ (9 mL min⁻¹) and steam (16 mL min⁻¹).

2.4. Analysis of products

The qualitative analysis of 3-methylindole was proceeded on a 500 superconducting NMR spectrometer of Bruker. The other products were qualitatively detected by Shimadzu QP2010 GC-MS instrument with DB-5MS, in which the temperature was changed from 373 to 533 K at a 15 K min⁻¹ temperature increasing rate. The reaction products were quantitatively determined by gas chromatography with HP-5 capillary column and N-hexanol was the internal standard.

Glycerol conversion, 3-methylindole yield or selectivity was calculated as follows:

$$\text{Conv. (\%)} = \frac{n_o - n_t}{n_o} \times 100\%$$

$$\text{Yield (\%)} = \frac{n_p}{n_o} \times 100\%$$

$$\text{Sel. (\%)} = \frac{\text{Yield}}{\text{Conv.}} \times 100\%$$

Here n_o or n_t was the amount of initial or final glycerol, respectively. And n_p was the amount of the target product.

2.5. Characterization of catalysts

The N₂ adsorption-desorption measurement of SBA-15 or its supported Ag-based catalyst was measured using a physical adsorption instrument of Micromeritics ASAP 2010 at 10⁻⁵ kPa, where the sample was evacuated and purify at 573 K for 3.0 h. The specific surface area of sample was calculated with the Brunauer-Emmett-Teller (BET) method. The relative pressure (P/P_0) of 0.05–0.30 was selected on the adsorption isotherm.

The mid-infrared analysis of sample was executed on the Nicolets50 Fourier transform infrared spectrometer. The scanning range was 2000–400 cm⁻¹.

The compositions of Ag/SBA-15-ZnO-CeO₂ were examined using field-emission scanning electron microscopy of Germany Carl Zeiss Supra55 with energy-dispersive X-ray spectroscopy (EDS) of UK Oxford X-MaxN. The acceleration voltage was 15 kV.

H₂-TPR measurement was proceeded in the 6 mm × 350 mm quartz tubular reactor. 100 mg catalyst precursor was filled and reactor was placed in the heating furnace connected to SP-6890a gas chromatograph with TCD detector. The sample was heated at 573 K in N₂ (30 mL

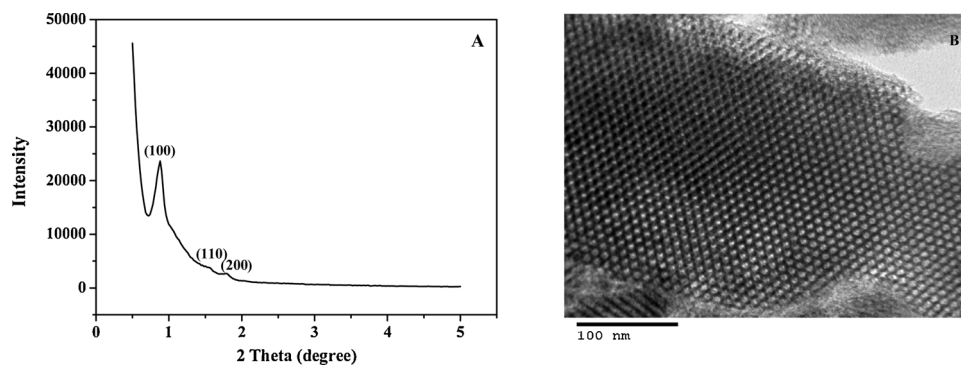


Fig. 1. XRD pattern (A) and TEM image (B) of the synthesized SBA-15 carrier.

min^{-1}) flow and purged at the temperature for 1.0 h to remove surface moisture and impurities, then lowered to 313 K. Finally the reduction was carried out in a mixed gas (30 mL min^{-1}) of H_2 -Ar ($V_{\text{H}_2}/V_{\text{Ar}}$ of 1/9) from 313 K to 873 K.

The crystal structures of SBA-15 carrier and Ag-based catalysts were detected on the Rigaku Smartlab 9 diffractometer using Cu-K α radiation with small-angle scanning range (2θ) from 0.5° to 5° and wide-angle scanning range (2θ) from 30° to 80° . Scan rates were $1^\circ/\text{min}$ and $5^\circ/\text{min}$, respectively. The tube current and tube voltage were 200 mA and 45 kV, respectively.

TEM study of SBA-15 carrier or SBA-15 supported Ag-based catalysts was proceeded on the JEM-2000EX microscope operated at an operating voltage of 50 kV. The sample was finely ground and sonicated for 0.5 h to make it fully dispersed in ethanol and then dripped on a porous grid for measurement.

The NH_3/CO_2 -TPD experimental device is the same as that of H_2 -TPR. Under He (35 mL min^{-1}) gas flow, a 150 mg of catalyst was heated from 293 K to 773 K ramping at 9.6 K min^{-1} , and held at 773 K for 1.0 h to remove impurities. Then the sample was adsorbed by NH_3 (or CO_2) at 373 K and purged at this temperature in He (35 mL min^{-1}) flow for 2.0 h. After that, the sample was heated to 973 K in a He gas flow (35 mL min^{-1}), and held at 973 K for 0.5 h.

The carbon deposition analyses for used catalysts were carried out on a 6300 Diamond TG-DTA thermogravimetric instrument of PerkinElmer. 7 mg of used catalyst was purged in a stream of nitrogen (20 mL min^{-1}) at 573 K, then lowered to 333 K, and maintained the temperature for 0.25 h. Following, the used catalyst was heated from 333 K to 1073 K with the air flow of 20 mL min^{-1} .

2.6. Regeneration of Ag/SBA-15-ZnO-CeO₂ catalyst

The deactivated catalyst sample of Ag/SBA-15-ZnO-CeO₂ was regenerated in a mixed gas (60 mL min^{-1}) of O_2 -N₂ ($V_{\text{O}_2}/V_{\text{N}_2}$ of 3/57) at 773 K for 4 h. Before the cycle reaction, the catalyst was reduced *in situ* at 453 K in a H_2 (15 mL min^{-1})-N₂ (15 mL min^{-1}) flow.

3. Results and discussion

3.1. Catalytic performance

The activity and selectivity of Ag/SBA-15 modified with ZnO and CeO₂ for the reaction of glycerol and aniline to synthesize 3-methylindole are shown in Tables 1 and 2. It can be observed from Table 1 that the conversion of glycerol was as low as 52% and the selectivity of 3-methylindole was only 25% over the catalyst of Ag/SBA-15. Both glycerol conversion and 3-methylindole selectivity increased remarkably when ZnO promoter was added to Ag/SBA-15. Additionally, with the content of ZnO increased, the selectivity of target product presented earlier increase and later decrease trend. When ZnO content was 1.00 mmol/g^{-1} , 3-methylindole yield reached 47%.

Table 1

The activity and selectivity of Ag/SBA-15-ZnO catalyst with different ZnO content.

ZnO content (mmol/g^{-1})	Glycerol conv. (%)	3-Methylindole yield (%)	3-Methylindole sel. (%)
0.00	52	13	25
0.60	82	40	49
0.80	86	44	51
1.00	89	47	53
1.20	91	43	47
1.40	93	40	43

Reaction conditions: 210°C , aniline:glycerol = 3:1 M ratio, $\text{SV} = 1700 \text{ h}^{-1}$, $\text{LHSV} = 0.4 \text{ h}^{-1}$, $\text{H}_2 = 15 \text{ mL/min}^{-1}$, steam = 16 mL/min^{-1} , $\text{N}_2 = 9 \text{ mL/min}$. Ag loading: 1.00 mmol/g^{-1} . The first hour results.

Table 2

The activity and selectivity of Ag/SBA-15-ZnO-CeO₂ catalyst with different CeO₂ content.

CeO ₂ content (mmol/g^{-1})	Glycerol conv. (%)	3-Methylindole yield (%)	3-Methylindole sel. (%)
0.00	89	47	53
0.02	87	53	61
0.03	86	57	66
0.04	85	60	71
0.05	83	62	75
0.06	82	59	72

Reaction conditions: 210°C , aniline:glycerol = 3:1 M ratio, $\text{LHSV} = 0.4 \text{ h}^{-1}$, $\text{SV} = 1700 \text{ h}^{-1}$, $\text{H}_2 = 15 \text{ mL/min}^{-1}$, steam = 16 mL/min^{-1} , $\text{N}_2 = 9 \text{ mL/min}$. Ag loading: 1.00 mmol/g^{-1} , ZnO content: 1.00 mmol/g^{-1} . The first hour results.

From Table 2 it can be seen that adding the promoter of CeO₂ to Ag/SBA-15-ZnO significantly increased the selectivity of 3-methylindole further, but glycerol conversion decreased slightly. And with increase of CeO₂ content, 3-methylindole selectivity also showed a tendency of firstly going up and then going down. When CeO₂ content was 0.05 mmol/g^{-1} , the optimal activity and selectivity were obtained with 3-methylindole yield up to 62%, which was higher than the best result [32].

Fig. 2 shows the 3-methylindole yield versus time on stream over SBA-15 supported Ag-base catalysts (Ag loading of 1.00 mmol/g^{-1} , the content of ZnO or CeO₂ of 1.00 or 0.05 mmol/g^{-1}). After adding the promoter of ZnO to Ag/SBA-15, the initial activity of the catalyst was improved observably. Continue to add CeO₂ promoter to Ag/SBA-15-ZnO, not only the activity was improved significantly, but also the deactivation of the catalyst was inhibited effectively, indicating that both ZnO and CeO₂ were the good promoters to improve the performance of the catalyst.

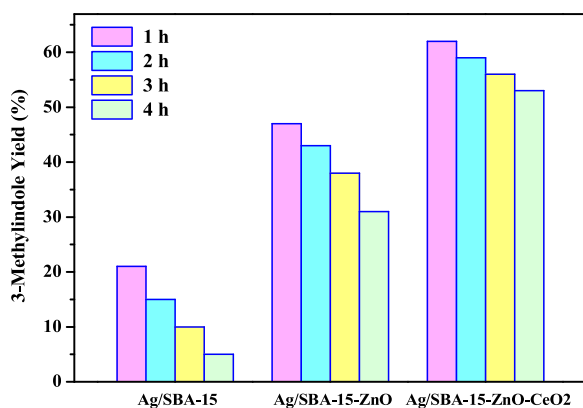


Fig. 2. The 3-methylindole yield versus time on stream over SBA-15 supported Ag-base catalysts.

Ag loading: 1.00 mmol/g^{-1} , ZnO content: 1.00 mmol/g^{-1} , CeO₂ content: 0.05 mmol/g^{-1}

3.2. Characterization of catalysts

3.2.1. N₂ physical adsorption

The N₂ adsorption-desorption isotherms, average pore width, specific surface areas and pore volume of SBA-15 and three Ag-based catalysts (Ag loading of 1.00 mmol/g^{-1} , the content of ZnO or CeO₂ of 1.00 or 0.05 mmol/g^{-1}) were shown in Fig. 3 and Table 3. From Fig. 3A it can be known that both SBA-15 and its supported silver-based catalysts exhibited typical IV isotherms with H1-type hysteresis loops, which indicates that these four samples existed mainly in mesoporous form [52]. From Fig. 3B it can be seen that there were two kinds of size distribution on SBA-15. The number of the mesopore at 3.63 nm was much more than the number of micropore at 1.36 nm . When Ag, ZnO and CeO₂ were loaded on SBA-15 successively, the number of micropore decreased clearly, while the number of mesopore obviously increased in sequence, and pore size gradually grew.

As it is obvious from Table 3, the specific surface area decreased with loading of Ag, ZnO and CeO₂ consecutively, indicated the presence of the active component on the SBA-15 framework as well as the promoters of ZnO and CeO₂. The pore volume of SBA-15 supported Ag-based catalysts increased a little after Ag, ZnO and CeO₂ were loaded on SBA-15 successively.

3.2.2. FT-IR

Fig. 4 shows the mid-infrared spectroscopic data of carrier and silver-based catalysts (Ag loading of 1.00 mmol/g^{-1} , the content of ZnO or CeO₂ of 1.00 or 0.05 mmol/g^{-1}). It can be seen that on the sample of SBA-15, there were absorbance peaks at 466 , 800 , 1091 , and

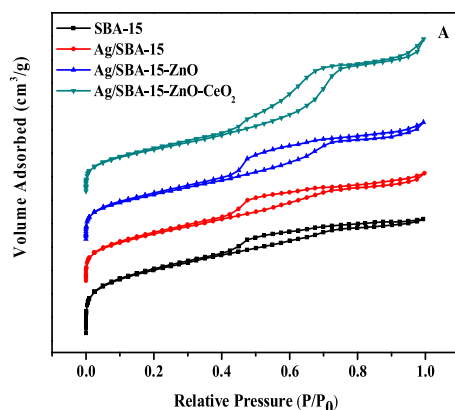


Fig. 3. N₂ adsorption-desorption isotherms (A) and pore size distribution (B) of SBA-15 and SBA-15 supported Ag-based catalysts. Ag loading: 1.00 mmol/g^{-1} , ZnO content: 1.00 mmol/g^{-1} , CeO₂ content: 0.05 mmol/g^{-1}

Table 3
Specific surface areas and pore volume of SBA-15 and SBA-15 supported Ag-based catalysts^a.

Sample	S _{BET} (m ² /g ⁻¹)	Pore volume (cm ³ /g ⁻¹)
SBA-15	521	0.543
Ag/SBA-15	406	0.558
Ag/SBA-15-ZnO	379	0.562
Ag/SBA-15-ZnO-CeO ₂	345	0.568

^a Ag loading: 1.00 mmol/g^{-1} , ZnO content: 1.00 mmol/g^{-1} , CeO₂ content: 0.05 mmol/g^{-1} .

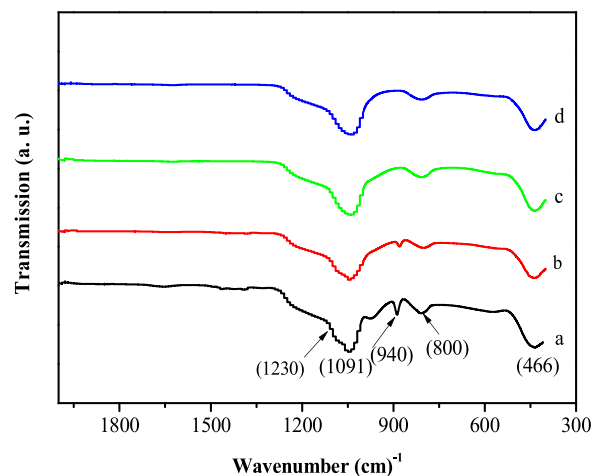


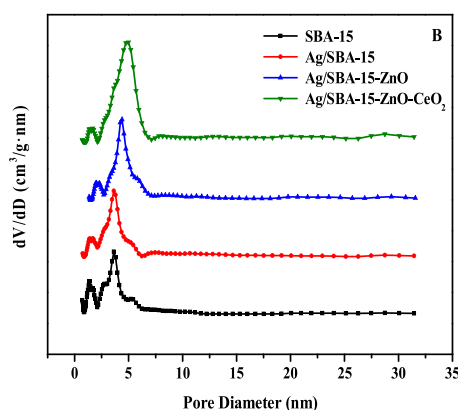
Fig. 4. Middle FT-IR spectra of SBA-15 (a), Ag/SBA-15 (b), Ag/SBA-15-ZnO (c) and Ag/SBA-15-ZnO-CeO₂ (d).

Ag loading: 1.00 mmol/g^{-1} , ZnO content: 1.00 mmol/g^{-1} , CeO₂ content: 0.05 mmol/g^{-1}

1230 cm^{-1} , attached to absorption vibration peaks of typical Si-O-Si [53,54], meanwhile an absorption peak of 940 cm^{-1} was observed, which belonged to winding vibration peak of Si-OH [55]. After SBA-15 was supported with Ag, ZnO and CeO₂, the bending vibration intensity of Si-OH weakened gradually, however the infrared absorption peaks at 466 , 800 , 1091 , and 1230 cm^{-1} still existed, indicating that the SBA-15 skeleton on the silver-based catalysts remained stable.

3.2.3. SEM-EDX

Fig. 5 presents the SEM-EDX mappings of Ag/SBA-15-ZnO-CeO₂ catalyst (Ag loading of 1.00 mmol/g^{-1} , the content of ZnO or CeO₂ of 1.00 or 0.05 mmol/g^{-1}) and the result adequately confirmed a presence of Ag, Zn or Ce in the sample of Ag/SBA-15-ZnO-CeO₂.



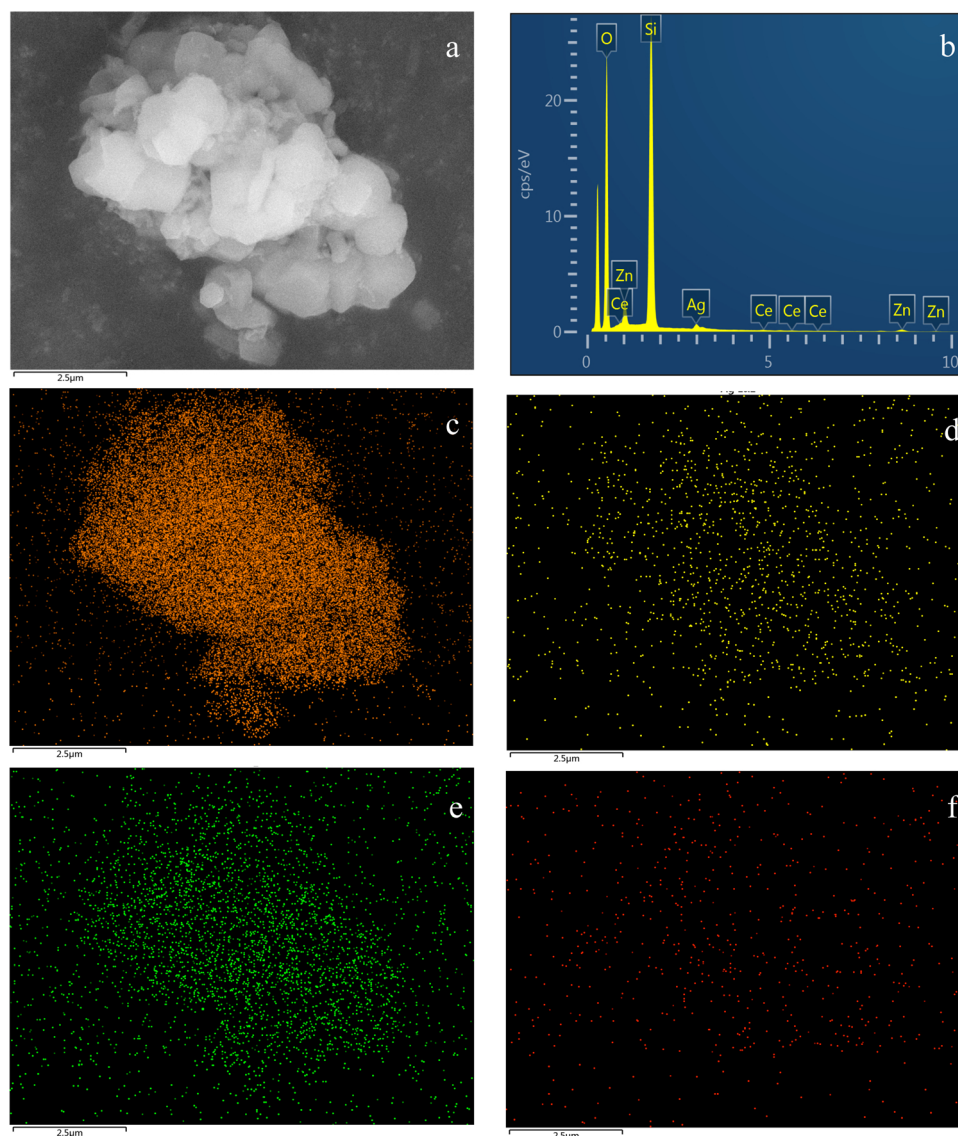


Fig. 5. SEM-EDX mappings of as-reduced Ag/SBA-15-ZnO-CeO₂ catalyst.

(a) dark-field image, (b) the EDX spectrum, (c→f) elemental SEM-EDX mapping images of the measured Si intensity, Ag intensity, Zn intensity and Ce intensity Ag loading: 1.00 mmol/g⁻¹, ZnO content: 1.00 mmol/g⁻¹, CeO₂ content: 0.05 mmol/g⁻¹

Moreover, the EDS mappings showed homogeneous distributions of the loaded metal ions, i.e., Ag, Zn and Ce.

3.2.4. H₂-TPR

H₂-TPR is known as a good method to study the effect of promoter on the interaction between active component and carrier. Fig. 6 shows the H₂-TPR results of the composite carrier SBA-15-ZnO, SBA-15-ZnO-CeO₂ and the samples of Ag₂O/SBA-15, Ag₂O/SBA-15-ZnO, Ag₂O/SBA-15-ZnO-CeO₂ (Ag₂O loading of 1.00 mmol/g⁻¹, the content of ZnO or CeO₂ of 1.00 or 0.05 mmol/g⁻¹). No hydrogen consumption peak was observed on SBA-15-ZnO or SBA-15-ZnO-CeO₂, indicating that ZnO and CeO₂ could not be reduced in the range of 373–643 K. When ZnO was added to Ag₂O/SBA-15, the reduction temperature of Ag₂O was significantly increased, suggesting that ZnO strengthened the interaction between the active component and the carrier, which brought about the reduction of Ag₂O difficult. After adding 0.05 mmol/g⁻¹ content of CeO₂ promoter to Ag₂O/SBA-15-ZnO, the reduction peak of Ag₂O obviously turned to a lower temperature, revealed that CeO₂ altered the electronic property of Ag₂O, which made Ag₂O acquire electrons more easily [56,57].

3.2.5. XRD

Fig. 7 presents XRD patterns of small angle (A) and wide angle (B) of a series fresh and used catalysts with Ag loading of 1.00 mmol/g⁻¹, the content of ZnO or CeO₂ of 1.00 or 0.05 mmol/g⁻¹, respectively. From Fig. 7A it can be observed that three diffraction peaks appeared at 2θ of 0.9, 1.6, and 1.9° on Ag/SBA-15 catalyst, assigning to the (100), (110), (200) reflections of SBA-15. Although the diffraction intensity turned to weak after the incorporation of ZnO and CeO₂ into Ag/SBA-15 catalyst in sequence no matter on the fresh or the used silver-based catalysts, the SBA-15 skeleton still remained. The conclusion was consistent with the FT-IR result in Fig. 4.

From Fig. 7B it can be observed that there were two silver crystal diffraction peaks at 2θ of 38.2° and 44.4° on Ag/SBA-15 catalyst in 30–60°, attributed to (111) and (220) crystal plane of silver [58]. After adding the promoter of ZnO to Ag/SBA-15, the diffraction peak distributed to (111) become very wide, while the peak assigned to (220) completely disappeared, revealed that ZnO promoter significantly improved the dispersion of Ag particles. After CeO₂ was added to Ag/SBA-15-ZnO, the intensity of the diffraction peak of silver increased a little, demonstrating that CeO₂ could not further promote the dispersion of Ag

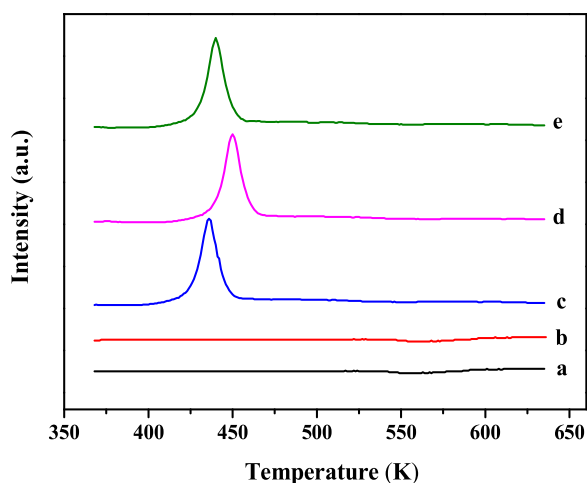


Fig. 6. H_2 -TPR profiles of SBA-15-ZnO (a), SBA-15-ZnO-CeO₂ (b), Ag₂O/SBA-15 (c), Ag₂O/SBA-15-ZnO (d) and Ag₂O/SBA-15-ZnO-CeO₂ (e). Ag₂O loading: 1.00 mmol/g⁻¹, ZnO content: 1.00 mmol/g⁻¹, CeO₂ content: 0.05 mmol/g⁻¹.

on the composite carrier of SBA-15-ZnO.

Comparing the XRD patterns on the fresh catalyst of Ag/SBA-15, the intensity of silver diffraction peak on the used catalyst of Ag/SBA-15 was significantly enhanced, indicating that a severe aggregation happened during the reaction. The aggregation of catalyst decreased obviously after adding ZnO to Ag/SBA-15, indicating that the promoter of ZnO could restrain the aggregation of Ag particles during the reaction effectively. CeO₂, however, could not play the function.

3.2.6. TEM

Fig. 8 is the TEM images and size distributions of Ag particles on the fresh and the used Ag-based catalysts with Ag loading of 1.00 mmol/g⁻¹, ZnO or CeO₂ content of 1.00 or 0.05 mmol/g⁻¹, respectively. It can be observed that the size of silver particles was ca. 14.1 nm on the fresh Ag/SBA-15. After adding 1.00 mmol/g⁻¹ of ZnO promoter to Ag/SBA-15, the average diameter of silver particles decreased to 4.8 nm, showing that ZnO improved silver dispersion greatly. When CeO₂ with the content of 0.05 mmol/g⁻¹ was added to the catalyst of Ag/SBA-15-ZnO, the average size of silver particles increased to 6.5 nm, revealed that doping CeO₂ did not improve the dispersion of active component silver, which was the same as the XRD result obtained in Fig. 7A.

Compared with the result in Fig. 8(a), silver particles on the used Ag/SBA-15 grew a lot with the average size up to 22.1 nm, indicating that a severe aggregation of active component occurred after 4.0 h of the reaction. When ZnO was added to Ag/SBA-15, the average size of

silver particles only increased to 7.7 nm at the same reaction time, illustrating that the addition of ZnO inhibited the aggregation of silver particles during the reaction effectively. This should be directly related to the fact that ZnO can enhance the interaction between active component and carrier. On the used Ag/SBA-15-ZnO-CeO₂ catalyst, the size of silver particles increased from 7.7 nm to 10.1 nm, indicating that the aggregation of silver particles increased slightly after adding the promoter of CeO₂ to Ag/SBA-15-ZnO. From Fig. 6 it can be known that adding the promoter of CeO₂ to Ag₂O/SBA-15-ZnO made Ag₂O be reduced more easily, suggested that CeO₂ could weaken the interaction between Ag₂O and the carrier, therefore the aggregation of active component silver occurred with ease.

3.2.7. NH₃/CO₂-TPD

Fig. 9 is the NH₃/CO₂-TPD data of silver-based catalysts with Ag loading of 1.00 mmol/g⁻¹, ZnO or CeO₂ content of 1.00 or 0.05 mmol/g⁻¹, respectively. It is obvious in Fig. 9A that the number of weak-acid centers assigned to the desorption peak of NH₃ below 473 K was fairly small on Ag/SBA-15, however the amount of medium-strong acid centers attributed to the desorption peak of NH₃ between 473 ~ 723 K was a lot. After doping the promoter of ZnO into Ag/SBA-15, the number of medium-strong acid centers decreased somewhat, but the number of weak-acid centers increased a lot, which led to a significant increase in the selectivity of the catalyst for 3-methylindole [33]. After CeO₂ promoter was added to Ag/SBA-15-ZnO, the number of weak-acid centers decreased slightly as well as the number of medium-strong acid centers, meanwhile the acidity of the catalyst was weakened for the peak of NH₃ attributed to medium-strong acid shifted to a lower temperature, which was beneficial to the reaction because carbon deposition could be suppressed correspondingly.

Fig. 9B demonstrates CO₂-TPD profiles of silver-based catalyst. On the three SBA-15 supported Ag-based catalysts, there was only one desorption peak of CO₂ belonged to medium-strong base. With the addition of ZnO promoter to Ag/SBA-15, not only the number of medium-strong base centers increased, but also the alkalinity enhanced. It was the addition of ZnO that increased the polarity (i.e. acidity and alkalinity) of SBA-15-ZnO composite carrier, so the interaction between silver and the carrier was heightened, as a result, the silver dispersion and sintering resistance of the catalyst were improved. When doping the promoter of CeO₂ to Ag/SBA-15-ZnO, the desorption peak of CO₂ obviously shifted to low temperature, revealed that the alkalinity of the catalyst weakened significantly.

3.2.8. TG-DTA

It is well known that acidity can bring about the formation of carbon deposition, which will obstruct the synthesis of 3-methylindole [59]. In order to know the formation of carbon deposition on catalyst during the reaction, the used Ag-based catalysts were characterized by TG-DTA

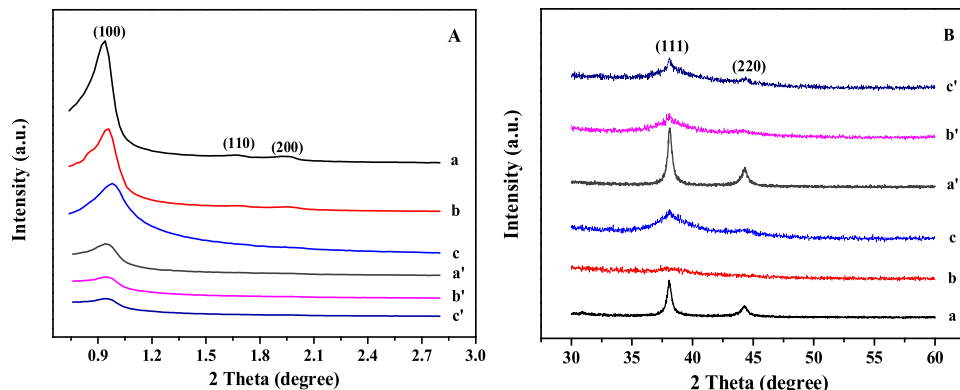


Fig. 7. XRD patterns of small angle (A) and wide angle (B) for the fresh and used Ag/SBA-15 (a, a'), Ag/SBA-15-ZnO (b, b') and Ag/SBA-15-ZnO-CeO₂ (c, c'). Ag loading: 1.00 mmol/g⁻¹, ZnO content: 1.00 mmol/g⁻¹, CeO₂ content: 0.05 mmol/g⁻¹.

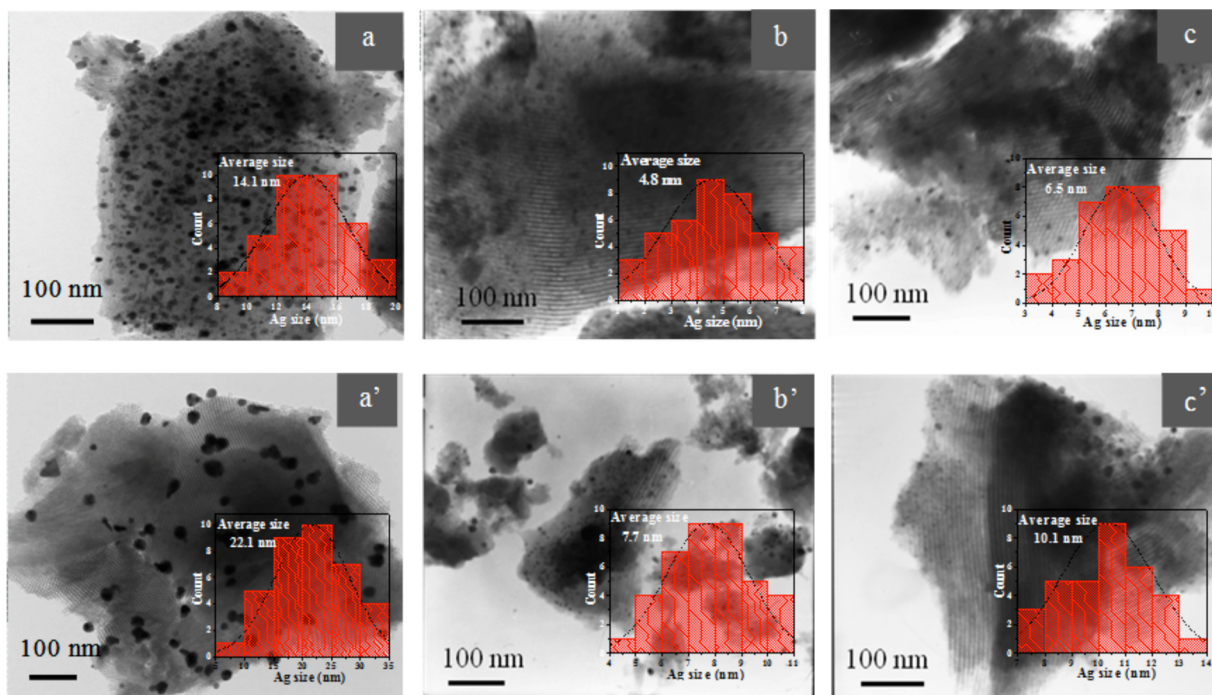


Fig. 8. TEM images and normal distributions of Ag particle size for the fresh and used Ag/SBA-15 (a, a'), Ag/SBA-15-ZnO (b, b') and Ag/SBA-15-ZnO-CeO₂ (c, c'). Ag loading: 1.00 mmol/g⁻¹, ZnO content: 1.00 mmol/g⁻¹, CeO₂ content: 0.05 mmol/g⁻¹

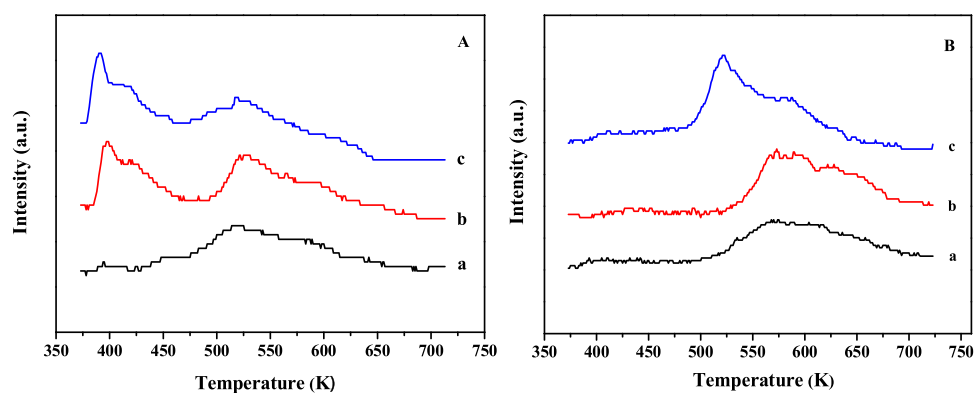


Fig. 9. NH₃-TPD (A) and CO₂-TPD (B) profiles of Ag/SBA-15 (a), Ag/SBA-15-ZnO (b) and Ag/SBA-15-ZnO-CeO₂ (c). Ag loading: 1.00 mmol/g⁻¹, ZnO content: 1.00 mmol/g⁻¹, CeO₂ content: 0.05 mmol/g⁻¹

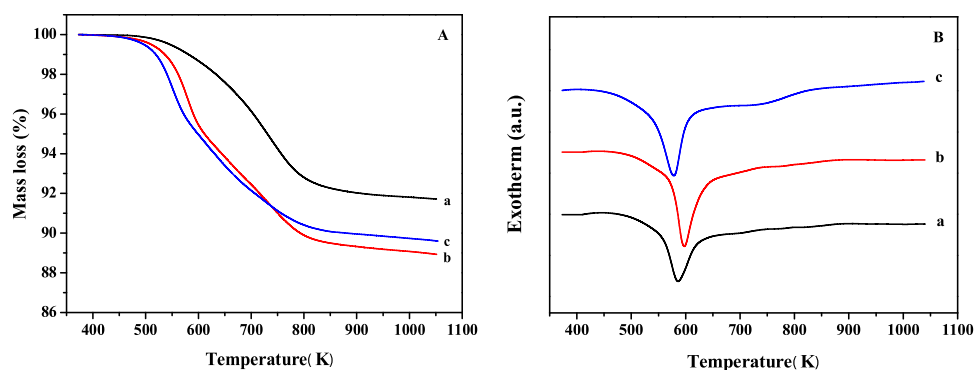


Fig. 10. TG(A)-DTA(B) results of the used Ag/SBA-15 (a), Ag/SBA-15-ZnO (b) and Ag/SBA-15-ZnO-CeO₂ (c). Ag loading: 1.00 mmol/g⁻¹, ZnO content: 1.00 mmol/g⁻¹, CeO₂ content: 0.05 mmol/g⁻¹

and Fig. 10 revealed the amount of carbon deposition and the degree to which carbon deposition can be oxidized. In Fig. 10A, an obvious mass loss existed on the used Ag/SBA-15, indicating the formation of carbon

deposition in the reaction. After adding the promoter of ZnO to Ag/SBA-15, the amount of carbon deposition increased, indicating that ZnO facilitated the formation of carbon deposition. It was undoubtedly due

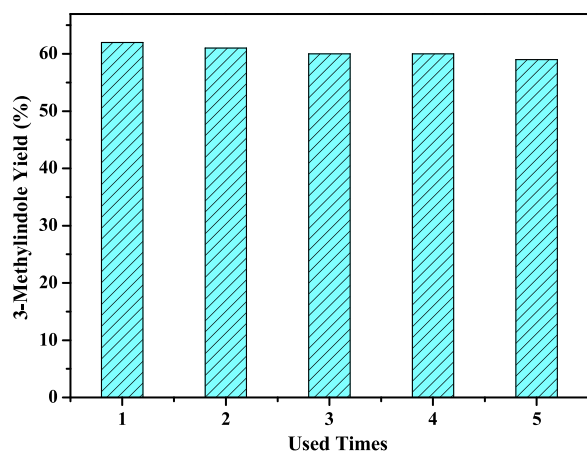


Fig. 11. Recycling activity of Ag/SBA-15-ZnO-CeO₂ catalyst. Ag loading: 1.00 mmol/g⁻¹, ZnO content: 1.00 mmol/g⁻¹, CeO₂ content: 0.05 mmol/g⁻¹

to the increased acidity of the catalyst after the addition of ZnO, and which was consistent with the NH₃-TPD result in Fig. 9A. The amount of carbon deposition decreased after adding the promoter of CeO₂ to Ag/SBA-15-ZnO, which was associated with the weakening of acidity of the catalyst after the addition of CeO₂. The same result can also be obtained from the DTA profiles in Fig. 10B. In addition, from the DTA exotherms on the used Ag-based catalysts it can be known that the carbon deposition was not easily oxidized after adding ZnO to Ag/SBA-15. The situation was modified a lot when CeO₂ was added to Ag/SBA-15-ZnO, indicating that the types of carbon deposition on the three used Ag-based catalysts were somewhat different.

3.3. Catalyst reusability

The Reusability of Ag/SBA-15-ZnO-CeO₂ (Ag loading of 1.00 mmol/g⁻¹, ZnO content of 1.00 mmol/g⁻¹, CeO₂ content of 0.05 mmol/g⁻¹) was tested. The catalyst underwent the regeneration after each run, and was reduced *in situ* again *prior* to activity test. From Fig. 11 it can be seen that only 3% of 3-methylindole yield declined when Ag/SBA-15-ZnO-CeO₂ was circulated five times, indicating that it had a good practicality.

3.4. Research on the reaction pathway

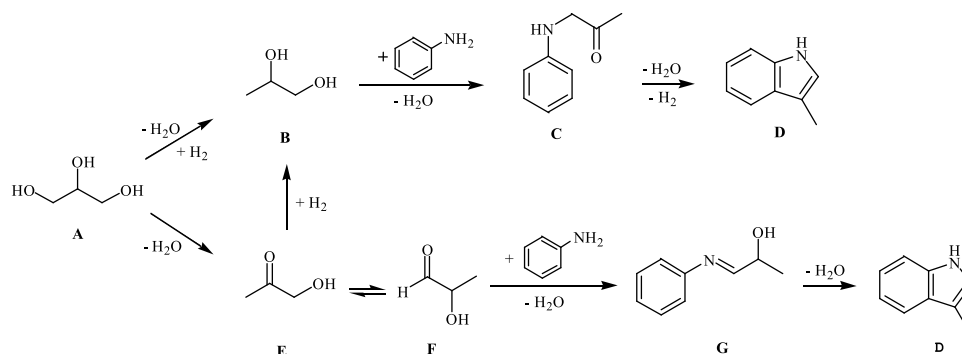
In recent years, we have conducted a meticulous investigation for the catalytic pathway of glycerol and aniline to 3-methylindole over copper-based catalysts [32,33]. Here, the reaction pathway for the reaction catalyzed by Ag/SBA-15-ZnO-CeO₂ catalyst was researched. From GC-MS analysis it was known that, except the main by-products of *N*-methylaniline, *p*-methylaniline, *N*-ethylaniline, *p*-ethylaniline,

acetol, etc., there was also a small number of 1,2-propanediol. Based on the reported literatures [60–63], 1,2-propanediol and acetol can be generated from glycerol, therefore, the catalytic hydrogenolysis of glycerol on SBA-15 supported silver-based catalyst was carried out. It was found that the main product was acetol, 1,2-propanediol was only a little. On the basis of literatures [64,65], 1,2-propanediol can also be formed from acetol, so the catalytic conversion of acetol was further proceeded on the catalyst and 1,2-propanediol was indeed found. Since 3-methylindole syntheses using 1,2-propanediol and aniline as raw materials over SiO₂ supported silver-based catalysts were achieved [66,67], the conversion reaction of 1,2-propanediol and aniline over Ag/SBA-15-ZnO-CeO₂ was carried out as well as the conversion of acetol with aniline and it was found that both the reactions could produce the objective product of 3-methylindole.

Based on the above experiments and literatures [33,68], a possible pathway to synthesize 3-methylindole in vapor-phase by glycerol with aniline over Ag/SBA-15-ZnO-CeO₂ catalyst was proposed as shown in Scheme 1. 1,2-Propanediol or acetol can be made from the hydrogenolysis or dehydration of glycerol. Some acetol could be converted into 1,2-propanediol by hydrogenation. 1,2-propanediol as well as acetol can be catalyzed with aniline to generate the target product of 3-methylindole, in which 1,2-propanediol reacted with aniline to form 1-phenylamino-acetone by dehydration, then produced the target product of 3-methylindole by dehydration and dehydrogenation [33], while acetol was firstly transformed to 2-hydroxy-1-propanal (F) via enol-keto tautomerism, and F reacted with aniline to generate 3-methylindole with 1-phenylimino-2-propanol as the intermediate [68].

4. Conclusion

3-Methylindole was efficiently synthesized in a low-cost and green way over Ag/SBA-15 modified with ZnO and CeO₂ using biomass-derived glycerol and aniline as raw materials. The catalyst exhibited a superior catalytic activity and selectivity, which a 62% yield and a 75% selectivity of 3-methylindole were obtained. A series of characterizations researches showed that the addition of ZnO promoter efficiently improved the dispersion of silver and inhibited the aggregation of Ag particles during the reaction because ZnO could increase the interaction between the silver and composite carrier. Adding the promoter of CeO₂ promoter to the Ag/SBA-15-ZnO catalyst could cut down the formation of carbon deposition in the reaction process. Furthermore, with adding the promoters of ZnO and CeO₂, the quantity of weak-acid centers of catalysts increased obviously, this contributed to achieve a higher selectivity of the target product. When Ag/SBA-15-ZnO-CeO₂ was circulated five times, the yield of 3-methylindole still reached 59%, indicating a good stability was obtained for the catalyst. Through the research on the reaction pathway, it was concluded that glycerol can be converted to acetol and 1,2-propanediol on the catalyst of Ag/SBA-15-ZnO-CeO₂, and they can both react with aniline to produce the important chemical of 3-methylindole.



Scheme 1. A possible pathway for the vapor-phase synthesis of 3-methylindole from glycerol and aniline over Ag/SBA-15-ZnO-CeO₂ catalyst.

Declaration of Competing Interest

The authors declare that they have no known competing financial interests or personal relationships that could have appeared to influence the work reported in this paper.

Acknowledgment

We are gratefully thankful to the financial supported by the National Natural Science Foundation of China (Grant No. 21576128).

References

- [1] S.S. Pang, Advances in thermochemical conversion of woody biomass to energy, fuels and chemicals, *Biotechnol. Adv.* 37 (2019) 589–597, <https://doi.org/10.1016/j.biotechadv.2018.11.004>.
- [2] G.M. Lari, G. Pastore, M. Haus, Y. Ding, S. Papadokostantakis, C. Mondelli, J. Pérez-Ramírez, Environmental and economical perspectives of a glycerol bio-refinery, *Energy Environ. Sci.* 11 (2018) 1012–1029, <https://doi.org/10.1039/c7ee03116e>.
- [3] H.F. Wu, Q.B. Liu, Z. Bai, G.X. Xie, J. Zheng, Performance investigation of a novel multi-functional system for power, heating and hydrogen with solar energy and biomass, *Energy Convers. Manage.* 196 (2019) 768–778, <https://doi.org/10.1016/j.enconman.2019.06.040>.
- [4] E.R. Mamat, M.S.M. Sani, K. Sudhakar, A. Kadarohman, R.E. Sardjono, An overview of higher alcohol and biodiesel as alternative fuels in engines, *Energy Rep.* 5 (2019) 467–479, <https://doi.org/10.1016/j.egyrs.2019.04.009>.
- [5] D. Gielen, F. Boshell, D. Saygin, M.D. Bazilian, N. Wagner, R. Gorini, The role of renewable energy in the global energy transformation, *Energy Strateg. Rev.* 24 (2019) 38–50, <https://doi.org/10.1016/j.esr.2019.01.006>.
- [6] D. Adu-Mensah, D. Mei, L. Zuo, Q. Zhang, J. Wang, A review on partial hydrogenation of biodiesel and its influence on fuel properties, *Fuel* 251 (2019) 660–668, <https://doi.org/10.1016/j.fuel.2019.04.036>.
- [7] S.N. Gebremariam, J.M. Marchetti, Economics of biodiesel production: review, *Energy Convers. Manage.* 168 (2018) 74–84, <https://doi.org/10.1016/j.enconman.2018.05.002>.
- [8] N. Razali, A.Z. Abdullah, Production of lactic acid from glycerol via chemical conversion using solid catalyst: a review, *Appl. Catal. A Gen.* 543 (2017) 234–246, <https://doi.org/10.1016/j.apcata.2017.07.002>.
- [9] A. Villa, N. Dimitratos, C.E. Chan-Thaw, C. Hammond, L. Prati, G.J. Hutchings, Glycerol oxidation using gold-containing catalysts, *Acc. Chem. Res.* 48 (2015) 1403–1412, <https://doi.org/10.1021/ar500426g>.
- [10] C.A.G. Quispe, C.J.R. Coronado, J.A. Carvalho Jr, Glycerol: production, consumption, prices, characterization and new trends in combustion, *Renew. Sust. Energ. Rev.* 27 (2013) 475–493, <https://doi.org/10.1016/j.rser.2013.06.017>.
- [11] S. Lopez-Pedrajas, R. Estevez, J. Schnee, E.M. Gaigneaux, D. Luna, F.M. Bautista, Study of the gas-phase glycerol oxidative dehydrogenation on systems based on transition metals (Co, Fe, V) and aluminium phosphate, *Mol. Catal.* 455 (2018) 68–77, <https://doi.org/10.1016/j.mcat.2018.05.020>.
- [12] N. Galy, R. Nguyen, H. Yalgin, N. Thiebault, D. Luat, C. Len, Glycerol in subcritical and supercritical solvents, *J. Chem. Technol. Biotechnol.* 92 (2017) 14–26, <https://doi.org/10.1002/jctb.5101>.
- [13] C. Len, F. Delbecq, C. Cara Corpas, E. Ruiz Ramos, Continuous flow conversion of glycerol into chemicals: an overview, *Synthesis* 50 (2017) 723–741, <https://doi.org/10.1055/s-0036-1591857>.
- [14] R.S. Varma, C. Len, Glycerol valorization under continuous flow conditions-recent advances, *Curr. Opin. Green Sustain. Chem.* 15 (2019) 83–90, <https://doi.org/10.1016/j.cogsc.2018.11.003>.
- [15] K. Suthagar, K. Shanthi, P. Selvam, Hydrogenolysis of glycerol over silica-supported copper-nanocatalyst: effect of precipitating-agent and copper metal-loading, *Mol. Catal.* 458 (2018) 307–316, <https://doi.org/10.1016/j.mcat.2017.11.035>.
- [16] S. Jeon, Y.M. Park, J. Park, K. Saravanan, H.-K. Jeong, J.W. Bae, Synergistic effects of Nb₂O₅ promoter on Ru/Al₂O₃ for an aqueous-phase hydrodeoxygenation of glycerol to hydrocarbons, *Appl. Catal. A Gen.* 551 (2018) 49–62, <https://doi.org/10.1016/j.apcata.2017.12.006>.
- [17] J. Ding, T. Ma, M. Cui, R. Shao, R. Guan, P. Wang, Gas phase dehydration of glycerol to acrolein over Cs_{2.5}H_{0.5}PW₁₂O₄₀/Zr-MCM-41 catalysts prepared by supercritical impregnation, *Mol. Catal.* 461 (2018) 1–9, <https://doi.org/10.1016/j.mcat.2018.09.021>.
- [18] Ö.D. Bozkurt, N. Bağlar, S. Çelebi, A. Uzun, Assessment of acid strength in sodium-exchanged resin catalysts: consequences on glycerol etherification with isobutene in batch and flow reactors, *Mol. Catal.* 466 (2019) 1–12, <https://doi.org/10.1016/j.mcat.2018.12.027>.
- [19] G. Parameswaram, P.S.N. Rao, A. Srivani, G.N. Rao, N. Lingaiah, Magnesia-ceria mixed oxide catalysts for the selective transesterification of glycerol to glycerol carbonate, *Mol. Catal.* 451 (2018) 135–142, <https://doi.org/10.1016/j.mcat.2017.12.006>.
- [20] A. Hejna, P. Kosmela, K. Formela, Ł. Piszczyk, J.T. Haponiuk, Potential applications of crude glycerol in polymer technology—current state and perspectives, *Renew. Sust. Energ. Rev.* 66 (2016) 449–475, <https://doi.org/10.1016/j.rser.2016.08.020>.
- [21] W. Sun, D.Y. Liu, H.Y. Zhu, L. Shi, Q. Sun, A new efficient approach to 3-methylindole: vapor-phase synthesis from aniline and glycerol over Cu-based catalyst, *Catal. Commun.* 12 (2010) 147–150, <https://doi.org/10.1016/j.catcom.2010.08.011>.
- [22] J.G. Yu, J.G. Xu, Z.Q. Yu, Y. Jin, J. Li, Y.W. Lv, A continuous-flow Fischer indole synthesis of 3-methylindole in an ionic liquid, *J. Flow Chem.* 7 (2017) 33–36, <https://doi.org/10.1556/1846.2017.00004>.
- [23] D.A. Vargas, L.J. Méndez, A.S. Cánepa, R.D. Bravo, Sulfated zirconia: an efficient and reusable heterogeneous catalyst in the Friedel-Crafts acylation reaction of 3-methylindole, *Catal. Lett.* 147 (2017) 1496–1502, <https://doi.org/10.1007/s10562-017-2057-x>.
- [24] S.J. Kong, J.B. Zhang, X. Li, H. Pan, D.Y. Guo, De novo biosynthesis of indole-3-ethanol and indole-3-ethanol acetate in engineered *Escherichia coli*, *Biochem. Eng. J.* 154 (2020) 107432, <https://doi.org/10.1016/j.bej.2019.107432>.
- [25] Y. Nishida, N. Takeda, K. Matsuno, O. Miyata, M. Ueda, Acylative coupling of amine and indole using chloroform as a carbonyl group, *Eur. J. Org. Chem.* 2018 (2018) 3928–3935, <https://doi.org/10.1002/ejoc.201800571>.
- [26] Y.C. Wan, Y.H. Li, C.X. Yan, M. Yan, Z.L. Tang, Indole: a privileged scaffold for the design of anti-cancer agents, *Eur. J. Med. Chem.* 183 (2019) 111691, <https://doi.org/10.1016/j.ejmech.2019.111691>.
- [27] M. Zakarianezhad, H.R. Masoodi, M. Shool, Further insight into the mechanism of the novel multicomponent reactions involving isoquinoline and dimethyl acetylenedicarboxylate in the presence of 3-methylindole: theoretical and experimental approach, *Int. J. Chem. Kinet.* 48 (2016) 770–778, <https://doi.org/10.1002/kin.21031>.
- [28] Y.H. Park, Y.P. Shi, B. Liang, C.A.D. Medrino, Y.H. Jeon, E. Torres, K. Uppal, L. Slutsker, D.P. Jones, High-resolution metabolomics to discover potential parasite-specific biomarkers in a Plasmodium falciparum erythrocytic stage culture system, *Malaria J.* 14 (2015) 122–131, <https://doi.org/10.1186/s12936-015-0651-1>.
- [29] C.A. Simoneau, A.M. Strohl, B. Ganem, One-pot synthesis of polysubstituted indoles from aliphatic nitro compounds under mild conditions, *Tetrahedron Lett.* 48 (2007) 1809–1811, <https://doi.org/10.1016/j.tetlet.2007.01.031>.
- [30] V. Kanchupalli, D. Joseph, S. Katukojvala, Pyridazine N-Oxides as precursors of metallocarbene: rhodium-catalyzed transannulation with pyrroles, *Org. Lett.* 17 (23) (2015) 5878–5881, <https://doi.org/10.1021/acs.orglett.5b03064>.
- [31] M. Campanati, P. Savini, A. Tagliani, A. Vaccari, Environmentally friendly vapour phase synthesis of alkylquinolines, *Catal. Lett.* 47 (1997) 247–250, <https://doi.org/10.1023/A:1019033811243>.
- [32] K.X. Ke, F.L. Wu, L.T. Ren, Y.B. Jiao, N. Xing, L. Shi, An efficient catalyst of Cu/MIL-101 modified with CeO₂ for the conversion of biomass-derived glycerol with aniline to 3-methylindole, *Catal. Commun.* 136 (2019) 105896, <https://doi.org/10.1016/j.catcom.2019.105896>.
- [33] Y.X. Cui, X.S. Zhou, Q. Sun, L. Shi, Vapor-phase synthesis of 3-methylindole from glycerol and aniline over zeolites-supported Cu-based catalysts, *J. Mol. Catal. A Chem.* 378 (2013) 238–245, <https://doi.org/10.1016/j.molcata.2013.06.015>.
- [34] E. Doustkhah, H. Mohtasham, M. Farajzadeh, S. Rostamnia, Y. Wang, H. Arandiyani, M.H.N. Assadi, Organosiloxane tunability in mesoporous organosilica and punctuated Pd nanoparticles growth: theory and experiment, *Microporous Mesoporous Mater.* 293 (2020) 109832, <https://doi.org/10.1016/j.micromeso.2019.109832>.
- [35] E. Doustkhah, H. Mohtasham, M. Hasani, Y. Ide, S. Rostamnia, N. Tsunoji, M. Hussein, N. Assadi, Merging periodic mesoporous organosilica (PMO) with mesoporous aluminosilica (Al/Si-PMO): a catalyst for green oxidation, *Mol. Catal.* 482 (2020) 110676, <https://doi.org/10.1016/j.mcat.2019.110676>.
- [36] T.B. Benzaquen, P.A. Ochoa Rodríguez, A.L. Cánepa, S.G. Casuscelli, V.R. Elías, G.A. Eimer, Heterogeneous Fenton reaction for the treatment of ACE in residual waters of pharmaceutical origin using Fe-SBA-15 nanocomposites, *Mol. Catal.* 30 (2018) 110239, <https://doi.org/10.1016/j.mcat.2018.11.010>.
- [37] A. Rodríguez-Gómez, F. Platero, A. Caballero, G. Colón, Improving the direct synthesis of hydrogen peroxide from hydrogen and oxygen over Au-Pd/SBA-15 catalysts by selective functionalization, *Mol. Catal.* 445 (2018) 142–151, <https://doi.org/10.1016/j.mcat.2017.10.034>.
- [38] R. Khatun, P. Bhanja, R.A. Molla, S. Ghosh, A. Bhaumik, S.M. Islam, Functionalized SBA-15 material with grafted-CO₂H group as an efficient heterogeneous acid catalyst for the fixation of CO₂ on epoxides under atmospheric pressure, *Mol. Catal.* 434 (2017) 25–31, <https://doi.org/10.1016/j.mcat.2017.01.013>.
- [39] M.C. Bacariza, I. Graça, S.S. Bebianno, J.M. Lopes, C. Henriques, Micro- and mesoporous supports for CO₂ methanation catalysts: a comparison between SBA-15, MCM-41 and USY zeolite, *Chem. Eng. Sci.* 175 (2018) 72–83, <https://doi.org/10.1016/j.ces.2017.09.027>.
- [40] X.D. Zhang, H. Dong, Z.J. Gu, G. Wang, Y.H. Zuo, Y.G. Wang, L.F. Cui, Preferential carbon monoxide oxidation on Ag/Al-SBA-15 catalysts: effect of the Si/Al ratio, *Chem. Eng. J.* 269 (2015) 94–104, <https://doi.org/10.1016/j.cej.2015.01.085>.
- [41] R.D. Andrei, N. Cambuzzi, M. Bonne, B. Lebeau, V. Hulea, Selective sulfoxidation reactions with H₂O₂ catalyzed by Ti-containing SBA-15 materials, *J. Porous Mater.* 26 (2018) 533–539, <https://doi.org/10.1007/s10934-018-0640-1>.
- [42] P. Rezaee, S. Elahi, J. Davarpanah, Synthesis of the organic-inorganic hybrid catalyst via covalently anchored basic organometallics on to the SBA-15: a recyclable catalyst for the preparation of chromene derivatives in water, *J. Porous Mater.* 26 (2018) 541–551, <https://doi.org/10.1007/s10934-018-0643-y>.
- [43] C.K.P. Neeli, H.P.R. Kannapu, V.N. Kalevaru, S.R.R. Kamaraju, D.R. Burri, An efficient and selective benzylic oxidation of tetralin to 1-tetralone on Cu(II) immobilized γ-Fe₂O₃@SBA-15 magnetic nanocatalyst in green water medium without base or additives, *Mol. Catal.* 453 (2018) 74–84, <https://doi.org/10.1016/j.mcat.2018.04.030>.
- [44] A. Rodríguez-Gómez, F. Platero, A. Caballero, G. Colón, Improving the direct synthesis of hydrogen peroxide from hydrogen and oxygen over Au-Pd/SBA-15 catalysts by selective functionalization, *Mol. Catal.* 445 (2018) 142–151, <https://doi.org/10.1016/j.mcat.2017.10.034>.

- doi.org/10.1016/j.mcat.2017.10.034.
- [45] V. Boosa, V. Bilakanti, V.K. Velisoju, N. Gutta, S. Inkolli, V. Akula, An insight on the influence of surface Lewis acid sites for regioselective C-H bond C₃-cyanation of indole using NH₄I and DMF as combined cyanide source over Cu/SBA-15 catalyst, *Mol. Catal.* 445 (2018) 43–51, <https://doi.org/10.1016/j.mcat.2017.11.007>.
- [46] C.P. Jiménez-Gómez, J.A. Cecilia, F.I. Franco-Duro, M. Pozo, R. Moreno-Tost, P. Maireles-Torres, Promotion effect of Ce or Zn oxides for improving furfuryl alcohol yield in the furfural hydrogenation using inexpensive Cu-based catalysts, *Mol. Catal.* 455 (2018) 121–131, <https://doi.org/10.1016/j.mcat.2018.06.001>.
- [47] S. Aghamohammadi, M. Haghghi, M. Maleki, N. Rahemi, Sequential impregnation vs. Sol-gel synthesized Ni/Al₂O₃-CeO₂ nanocatalyst for dry reforming of methane: effect of synthesis method and support promotion, *Mol. Catal.* 431 (2017) 39–48, <https://doi.org/10.1016/j.mcat.2017.01.012>.
- [48] I. Kaskow, I. Sobczak, M. Ziolk, V.C. Corberán, The effect of support properties on n-octanol oxidation performed on gold–silver catalysts supported on MgO, ZnO and Nb₂O₅, *Mol. Catal.* 2 (2019) 110674, <https://doi.org/10.1016/j.mcat.2019.110674>.
- [49] P. Yang, J. Li, S. Zuo, Promoting oxidative activity and stability of CeO₂ addition on the MnO_x modified kaolin-based catalysts for catalytic combustion of benzene, *Chem. Eng. Sci.* 162 (2017) 218–226, <https://doi.org/10.1016/j.ces.2017.01.009>.
- [50] D. Zhao, Q. Huo, J. Feng, B.F. Chmelka, G.D. Stucky, Nonionic triblock and star diblock copolymer and oligomeric surfactant syntheses of highly ordered, hydrothermally stable, mesoporous silica structures, *J. Am. Chem. Soc.* 120 (1998) 6024–6036, <https://doi.org/10.1021/ja506344k>.
- [51] J. Deng, L. Zhang, H. Dai, C.T. Au, In situ hydrothermally synthesized mesoporous LaCoO₃/SBA-15 catalysts: high activity for the complete oxidation of toluene and ethyl acetate, *Appl. Catal. A Gen.* 352 (2009) 43–49, <https://doi.org/10.1016/j.apcata.2008.09.037>.
- [52] A.S. Al-Fatesh, Y. Arafat, A.A. Ibrahim, H. Atia, A.H. Fakeeha, U. Armbruster, A.E. Abasaeed, F. Frusteri, Evaluation of Co-Ni/Sc-SBA-15 as a novel coke resistant catalyst for syngas production via CO₂ reforming of methane, *Appl. Catal. A Gen.* 567 (2018) 102–111, <https://doi.org/10.1016/j.apcata.2018.09.012>.
- [53] F. Chang, J. Wang, J. Luo, J. Sun, X. Hu, Synthesis, characterization, and visible-light-driven photocatalytic performance of W-SBA15, *J. Colloid Interface Sci.* 468 (2016) 284–291, <https://doi.org/10.1016/j.jcis.2016.01.077>.
- [54] F.H. Liu, J. Yu, G.Y. Tu, L. Qu, J.C. Xiao, Y.D. Liu, L.Z. Wang, J.Y. Lei, J.L. Zhang, Carbon nitride coupled Ti-SBA15 catalyst for visible-light-driven photocatalytic reduction of Cr (VI) and the synergistic oxidation of phenol, *Appl. Catal. B* 201 (2017) 1–11, <https://doi.org/10.1016/j.apcatb.2016.08.001>.
- [55] X.G. Wang, K.S.K. Lin, J.C.C. Chan, S. Heng, Direct synthesis and catalytic applications of ordered large pore aminopropyl-functionalized SBA-15 mesoporous materials, *J. Phys. Chem. B* 109 (2005) 1763–1769, <https://doi.org/10.1021/jp045798d>.
- [56] X.S. Liu, X.D. Wu, D. Weng, L. Shi, Modification of Cu/ZSM-5 catalyst with CeO₂ for selective catalytic reduction of NO_x with ammonia, *J. Rare Earths* 34 (2016) 1004–1009, [https://doi.org/10.1016/s1002-0721\(16\)60127-8](https://doi.org/10.1016/s1002-0721(16)60127-8).
- [57] S.H. Lu, F. Wang, C.C. Chen, F.L. Huang, K.L. Li, Catalytic oxidation of formaldehyde over CeO₂-Co₃O₄ catalysts, *J. Rare Earths* 35 (2017) 867–874, [https://doi.org/10.1016/s1002-0721\(17\)60988-8](https://doi.org/10.1016/s1002-0721(17)60988-8).
- [58] J. Liu, X. Li, Q. Zhao, J. Ke, H. Xiao, X. Lv, S. Liu, M. Tadé, S. Wang, Mechanistic investigation of the enhanced NH₃-SCR on cobalt-decorated Ce-Ti mixed oxide: in situ FTIR analysis for structure-activity correlation, *Appl. Catal. B* 200 (2017) 297–308, <https://doi.org/10.1016/j.apcatb.2016.07.020>.
- [59] S.S. Gao, S.T. Xu, Y.X. Wei, Q.L. Qiao, Z.C. Xu, X.Q. Wu, M.Z. Zhang, Y.L. He, S.L. Xu, Z.M. Liu, Insight into the deactivation mode of methanol-to-olefins conversion over SAPO-34: coke, diffusion, and acidic site accessibility, *J. Catal.* 367 (2018) 306–314, <https://doi.org/10.1016/j.jcat.2018.09.010>.
- [60] A.K. Kinage, P.P. Upare, P. Kasinathan, Y.K. Hwang, J.-S. Chang, Selective conversion of glycerol to acetol over sodium-doped metal oxide catalysts, *Catal. Commun.* 11 (2010) 620–623, <https://doi.org/10.1016/j.catcom.2010.01.008>.
- [61] F.F. Cai, F.K. Jin, J. Hao, G.M. Xiao, Selective hydrogenolysis of glycerol to 1,2-propanediol on Nb-modified Pd–Zr–Al catalysts, *Catal. Commun.* 131 (2019) 105801, <https://doi.org/10.1016/j.catcom.2019.105801>.
- [62] C.H. Zhou, K. Deng, M.D. Serio, S. Xiao, D.S. Tong, L. Li, C.X. Lin, J. Beltramini, H. Zhang, W.H. Yu, Cleaner hydrothermal hydrogenolysis of glycerol to 1,2-propanediol over Cu/oxide catalysts without addition of external hydrogen, *Mol. Catal.* 432 (2017) 274–284, <https://doi.org/10.1016/j.mcat.2017.02.008>.
- [63] T. Gabrys, M. Muhler, B. Peng, The kinetics of glycerol hydrodeoxygenation to 1,2-propanediol over Cu/ZrO₂ in the aqueous phase, *Appl. Catal. A Gen.* 576 (2019) 47–53, <https://doi.org/10.1016/j.apcata.2019.03.001>.
- [64] V. Montes, M. Checa, A. Marinas, M. Boutonnet, J.M. Marinas, F.J. Urbano, S. Järas, C. Pinel, Synthesis of different ZnO-supported metal systems through microemulsion technique and application to catalytic transformation of glycerol to acetol and 1,2-propanediol, *Catal. Today* 223 (2014) 129–137, <https://doi.org/10.1016/j.cattod.2013.09.021>.
- [65] T. Miyazawa, S. Koso, K. Kunimori, K. Tomishige, Glycerol hydrogenolysis to 1,2-propanediol catalyzed by a heat-resistant ion-exchange resin combined with Ru/C, *Appl. Catal. A Gen.* 329 (2007) 30–35, <https://doi.org/10.1016/j.apcata.2007.06.019>.
- [66] J.C. Zheng, J. Liu, W. Tan, L. Shi, Q. Sun, Vapor phase synthesis of 3-methylindole over a Ag/SiO₂ catalyst, *J. Chin. Catal.* 29 (2008) 1199–1201, [https://doi.org/10.1016/S1872-2067\(09\)60025-5](https://doi.org/10.1016/S1872-2067(09)60025-5).
- [67] W.H. Lü, Xh. Liu, D.Y. Liu, L. Shi, Q. Sun, Vapor-phase synthesis of 3-methylindole over Fe-, Co-, or Ni-promoted Ag/SiO₂ catalysts, *J. Chin. Catal.* 30 (2009) 1287–1290, [https://doi.org/10.1016/S1872-2067\(08\)60145-X](https://doi.org/10.1016/S1872-2067(08)60145-X).
- [68] M. Campanati, S. Franceschini, O. Piccolo, A. Vaccari, Reaction pathway in the vapour-phase synthesis of indole and alkylindoles, *J. Catal.* 232 (2005) 1–9, <https://doi.org/10.1016/j.jcat.2005.02.014>.